IEEE Access
Multidisciplinary | Rapid Review | Open Access Journal

Received March 20, 2022, accepted April 29, 2022, date of publication May 5, 2022, date of current version May 11, 2022.

Digital Object Identifier 10.1109/ACCESS.2022.3172963

General Aviation Aircraft Identification at Non-Towered Airports Using a Two-Step Computer Vision-Based Approach

MOHAMMAD FARHADMANESH, ABBAS RASHIDI, (Member, IEEE), AND NIKOLA MARKOVIĆ

Department of Civil and Environmental Engineering, The University of Utah, Salt Lake City, UT 84112, USA

Corresponding author: Mohammad Farhadmanesh (mohammad.farhadmanesh@utah.edu)

This work was supported in part by the Utah Department of Transportation (UDOT) under Grant UT20.605, in part by Mountain-Plains Consortium (MPC) under Grant MPC-639, and in part by the Airport Cooperative Research Program (ACRP).

ABSTRACT Aircraft identification in airport operations is critical to various applications, including airport planning and environmental studies. Previous research and commercially available systems heavily rely on recognizing aircraft tail numbers using text recognition. However, this approach alone does not provide accurate results in situations when the tail number visibility is reduced or obstructed. Furthermore, general aviation aircraft are harder to identify because they are small in size, and their tail numbers include substantial variations in fonts, sizes, and orientations. To tackle these issues, we propose a two-step computer vision-based aircraft identification method, which first identifies the aircraft type and then recognizes the tail number in a probabilistic multi-frame-based (MFB) framework. In the first step, a convolutional neural network (CNN)-based aircraft classifier is customized to decrease the search space in the registration database. In the second step, the identification process is finalized by integrating the text recognition results into the designed probabilistic MFB framework. The proposed method achieves approximately 90% identification accuracy when tested on video data collected from three general aviation airports. This is a significant improvement compared to text recognition alone, which recognizes 67% of the individual tail number characters.

INDEX TERMS Intelligent transportation systems, computer vision, airports, aircraft.

I. INTRODUCTION

Airport operations data is critical for preparing master plans and fair allocation of state and federal funds [1]. Also, operations data facilitates environmental studies investigating the negative effects on the surrounding communities [2]. While air traffic control (ATC) towers provide detailed information about operating aircraft, more than 97% of the United States airports are not equipped with control towers [3]. These airports typically host general aviation and, in addition to corporate and self-piloted flights, provide the public with vital services, such as aerial firefighting, law enforcement, and aeromedical flights [4], [5]. Accordingly, several attempts have been made to automatically identify operating aircraft, including transponder-based methods. However, they exhibit limited accuracy and require aircraft to be equipped with transponders. Alternatively, computer vision has shown to be effective for intelligent transportation systems [6], especially airports [7], [8]. Moreover, a vision-based approach for aircraft identification can provide additional functionalities, such as billing landing fees and preventing runway incursion.

Previous studies have used computer vision to assist control towers with identifying airliners on the airfield surface [9]–[11]. Similarly to commercially available applications, they merely use optical character recognition (OCR) techniques to identify the aircraft registration number (i.e., tail number) imprinted on the aircraft fuselage, which follow the International Civil Aviation Organization (ICAO) and Federal Aviation Administration (FAA) regulations [12]. However, the presented approaches have drawbacks in identifying ''difficult-to-read'' tail numbers. Specifically, general aviation aircraft are considerably smaller than airliners and exhibit more variation in their shape. They comprise more than 90% of the registered civil aviation aircraft in the U.S. [13] and also account for the operations of most non-towered airports. Their imprinted tail numbers exhibit

The associate editor coordinating the review of this manuscript and approving it for publication was Zhenbao Liu.

much variation in font, size, position, and orientation due to the lack of strict regulations compared to passenger airliners. Moreover, the visibility of tail numbers may be seriously affected by adverse lighting conditions. Accordingly, to overcome these challenges, this paper makes the following contributions:

- We propose a two-step aircraft identification method that classifies the aircraft before recognizing its tail number. To integrate the identification system with the FAA registration database, we classify aircraft based on the available visual information in the database (e.g., aircraft and engine type). We explore transfer learning and customize a convolutional neural network (CNN) architecture to obtain the best classifier. The proposed approach improves system accuracy by disregarding irrelevant tail numbers from the database and by finding the class of operating aircraft for miss-identified cases.
- We design a probabilistic multi-frame-based (MFB) framework to finalize the identification results. It uses the results of a text recognition network in a sequence of video frames and transforms them into a probabilistic tail number identification. Additionally, we propose a fast tail number detector using a cascaded feature-based approach to reduce the computing times and enable real-time applications.
- We publish the collected test dataset from the airfield of three general aviation airports in Utah containing video frames of operating aircraft with annotation text files for aircraft and its tail number to facilitate future studies and comparisons of algorithms [14].

The remainder of the paper is organized as follows. We first review the literature and then elaborate on the proposed method. Next, we discuss the system setup and report its accuracy on the collected data. Lastly, we discuss the limitations of the system and conclude the paper.

II. LITERATURE REVIEW

Acoustic, radio, and satellite-based methods are used to measure aircraft operations at non-towered airports. However, acoustic-based [15] and radio-based (i.e., general audio recording) [16] systems are incapable of identifying the aircraft. Mott [17] proposed a satellite-based method to detect airport flight activities by encoding the signal transmitted by a transponder carried by aircraft. This method utilizes the Automatic Dependent Surveillance-Broadcast (ADS-B) system. Mode A/C and Mode S aircraft transponder signals are common for civilian use. Only in Mode S signals, each aircraft is assigned a fixed ICAO 24-bit address that can match with aircraft registration in the FAA database (aircraft identity) [18]. Nevertheless, this system is currently inefficient due to the low equipage rate of the general aviation fleet with transponders (about 65% [19]). In addition, many of the general aviation aircraft in the U.S. (approximately 84% [20]) do not have transponders capable of transmitting Mode S signals that contain aircraft identity information. Consequently, this system cannot identify even a large portion of the equipped aviation fleet. A vision-based system can properly address this issue as it is a passive system and not limited to cooperative aircraft only.

Another advantage of a vision-based system are additional applications in the areas of safety and security. For example, the recognized visual information about the airfield can be used to signalize flight clearance for pilots approaching the airport. It would reduce runway incursion risk, which is a major safety concern (e.g., more than 1,511 runway incursions were reported in the last year alone [21]). Identifying unauthorized landings is another useful application of a vision-based system.

A. VISION-BASED METHODS

1) AIRCRAFT CLASSIFICATION

The image-based approach for measuring the aircraft operations presented in [22], [23] focuses on counting the operations. Another research line is the image classification methods to find the aircraft type or model. Image features like SIFT and SURF are used to detect and classify aircraft [24]. The deep learning approach has provided an end-to-end solution for automatic feature extraction for image classification [25]. Neural networks have also been extensively used for aircraft classification in remote sensing images [26]–[28]. Nonetheless, remote sensing image classification models cannot be used for airport-level operation monitoring systems because of the different camera fields of view. The closer range of view at airports can help us recognize the differences between similar aircraft models. Van Phat *et al.* [29] use deep neural networks for classifying two airliner classes (B737 and B767). Saghafi *et al.* [30] evaluate multi-layer neural networks for classifying aircraft via simulated training data using photos from 3D aircraft models (helicopters and propellers). Likewise, Ali and Choudhry [31] classify civil airliners using feedforward neural networks for video docking systems. Their developed models can classify a small range of the aircraft type/models, while operations at general aviation airports include a wide range of aircraft from propellers to jet airliners. Maji *et al.* [32] introduce a fine-grained aircraft image dataset that has been used for testing image-based fine-grained category recognition models using neural/non-neural techniques [33]. However, these proposed models focus on the classification of aircraft and cannot recognize the identity of individual aircraft, which can reveal detailed and necessary information (i.e., owner, technical information on aircraft registration, etc.).

This paper uses aircraft classification prior to tail number recognition to decrease the search space in the aircraft registration database and increase the aircraft identification accuracy. Therefore, a novelty of our work is the development of a classifier that is customized to leverage the FAA database as well as the visually perceivable information about the registered aircraft in that database (sections III-A and IV-A1). We use the HyperBand algorithm to enhance the performance of our customized classifier, which attains a comparable or

even better classification accuracy compared to its larger transferred deep learning model counterparts, ResNet50 [34] and Xception [35]. The developed classifier includes all types of aircraft included in the FAA database and is also tested and proven effective on video data collected from three general aviation airports.

Extensive research has focused on detecting airliners in commercial primary airports' video footages [9], [36]. Nevertheless, only a handful of articles paid attention to vision-based aircraft identification, while focusing exclusively on *airliners* using merely OCR methods. Next, we review existing articles and explain the differences and novelties of our proposed approach.

2) TAIL NUMBER RECOGNITION

Airliner identification methods via tail number recognition are studied by Molina *et al.* [10] and Vidakis and Kosmopoulos [11]. Their methods target surface movements in the airport terminal area. The image-based system developed in [10] (their results are also presented in [37], [38]) processes the manually selected images captured from slow-moving airliners in the terminal area. To localize the tail number zone in [10], the authors assume that the image histogram is distinctive in the region of interest (i.e., tail number) because of its high contrast with the local background, which helps them narrow down the search for tail numbers in images. However, in the case of smaller aircraft models, the fuselage size requires a close arrangement of different elements, including the tail number, windows, aircraft wing, and aircraft tail, which induces much more variations in the histograms of the subwindows of the aircraft image. In addition, in their proposed method, Molina *et al.* [10] focus on developing a custom OCR model that is sensitive to the spatial transformation of the characters. As a result, their method cannot be applied to smaller aircraft. There is a significant difference in the appearance of tail numbers imprinted on airliners and general aviation aircraft due to the lack of strict regulation for smaller aircraft. Generally, smaller aircraft have a more challenging tail number shape for visual recognition. These challenges stem from the higher variations in sizes, fonts, baseline orientations, and overall design of the smaller aircraft tail numbers.

Vidakis and Kosmopoulos [11] find the target video frame that contains the airliner tail (i.e., fin), assuming the vicinity of the tail and tail number. In the proposed method, a sliding window searches the image part close to the airliner tail, which is detected using blob analysis after background-foreground extraction (i.e., motion-based detection). Subsequently, the most frequently recognized number is introduced as the associated tail number to the taxiing aircraft in the apron area. This approach is inefficient for the following reasons: 1) It is computationally expensive to execute OCR over a large number of sliding windows; 2) The proposed approach is prone to identification-related errors as many sliding windows are not associated with the aircraft tail number; 3) there are many visual distractions in the actual video footage of operating aircraft, such as airport service vehicles, construction equipment, and nearby traffic, thus making the motion-based detections inefficient. 4) The author's assumption regarding the aircraft tail structure shape is not applicable to the smaller aircraft body shape configuration.

Similar to approaches proposed in [10], [11], [39], the commercially available applications (Vantage[1] [40] and Vax-OCR[2] [41]) for identifying aircraft focus on recognition of the aircraft tail number using OCR techniques. As a result, their approach will be limited in cases of difficult-to-read tail numbers and where the tail number visibility is affected by illumination. To overcome these challenges, we propose a two-step identification method and add a layer of classification by processing the visual information from the aircraft silhouette shape (using CNN-based classifiers) prior to tail number recognition (using text recognition) together with the FAA database to finalize the aircraft identification. Using the designed probabilistic MFB framework, we enhanced the system's reliability. In addition, we imposed a limit on the computational intensity of our algorithms to achieve a real-time system.

III. METHODOLOGY

Fig. 1 illustrates a schematic flowchart of the proposed two-step vision-based method for automatically identifying operating aircraft from video data. Any motion detected by background analysis triggers the system. It could be airport ground vehicles, personnel, nearby highway traffic, construction equipment, and animals. Next, we use Single Shot Detector (SSD) to detect operating aircraft and a fast correlation-based object tracker, Minimum Output Sum of Squared Error (MOSSE), to track the aircraft in the rest of the video frames. The built trajectory is further processed to count and recognize the type of aircraft activity (i.e., departure and landing). The system builds a recognition data bank for identifying the target aircraft by using a CNN-based classifier to detect the aircraft class and by recognizing the possible sequences associated with the aircraft tail number at selected video frames. The operation time windows vary between half a second and ten seconds. During this time, pilot maneuvers during take-off or landing might cause some distortion or occlusion of the tail number (e.g., due to the tilted aircraft fuselage). Thus, we extract video frames every 0.1 seconds from the collected aircraft operations footage. This ensures sufficient video frames to minimize the possibility of missing the tail number and maintains a real-time system considering the algorithms' processing times.

A CNN-based classifier uses the aircraft image box as input to perform the first step, find the aircraft class, and essentially remove the irrelevant candidates in the registration database. Subsequently, a tail number detector searches over the aircraft image box to localize and extract the tail number

[1]https://www.vector-us.com/vantage
[2]https://www.vaxtor.com/products/vaxocr/tailfin/

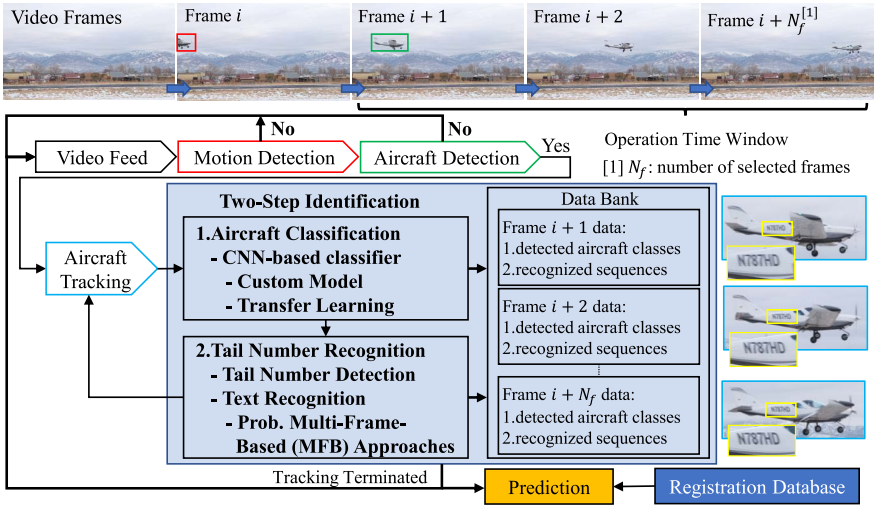

FIGURE 1. Aircraft identification system flowchart.

image to be used as an input of the text recognition algorithm in the second step. The departure of the aircraft from the camera field of view terminates tracking, and the aircraft identity will be predicted using three probabilistic MFB approaches by processing the data accumulated in the data bank and the registration database.

A. AIRCRAFT CLASSIFICATION

This module serves as a refinement filter to assist the identification process by reducing the search space for finding the associated tail number in the aircraft registration database. Specifically, it eliminates the tail numbers that are irrelevant to the recognized aircraft class. Aircraft classification can also alleviate the possible tail number miss-identifications by closely estimating the operating aircraft class information.

We test two common approaches for constructing a CNN-based classifier: (1) building a *custom model* from scratch and (2) *transfer learning*. The former has more flexibility in terms of optimizing the arrangement of the neurons in a convolutional layer pattern. The latter is more common among engineers because it yields a consistent performance, especially for cases with limited training data. To obtain a real-time aircraft identification system, we pay particular attention to classification speed and accuracy when assembling different models. Notably, the number of parameters influences the speed and accuracy of a CNN model.

1) CUSTOMIZED CNN-BASED CLASSIFIER MODEL

Fig. 2 demonstrates the architecture of the customized CNN for the aircraft classifier by optimizing the arrangement of layers. In this optimization problem, we fixed 5 convolutional blocks (denoted as Conv B) and 3 fully connected layers as the building blocks of our custom CNN-based classifier. Next, we apply the HyperBand algorithm [42] embedded in Keras [43] to tune and optimize the following parameters of those building blocks:

- **The number of convolutional layers in each block** is bounded to 1, 2, 3, 4, or 5.
- **Output dimensionality of each convolutional layer** is bounded to 16-64 for B1 layers, 32-128 for B2 layers, 64-256 for B3 layers, 128-512 for B4 and B5 layers (step sizes equal to lower bounds).
- **Output dimensionality of the first two fully connected layers** is bounded to 512-1024 for FC1 and 256-512 for FC2 (step sizes equal to half of the lower bounds).
- **Learning rate of the optimizer** is selected from {5e-3, 1e-3, 5e-4, 1e-4, 5e-5}.

The mentioned boundaries are determined experimentally for an optimized recognition performance. In each block, the set of convolutional layers (all with 3×3 kernels) is followed by a batch normalization layer to accelerate the training process (as suggested in [44]) and a max pooling layer to reduce the number of parameters progressively. The rectified linear unit (ReLU) function is assigned to calculate the output of the convolutional layers and the first two fully connected layers. At the top of the network, a softmax function is set to compute the probability of each aircraft class using the products of the last fully connected layer.

2) TRANSFERRED CNN-BASED CLASSIFIER MODELS

Here, we take a CNN model that is previously trained on the ImageNet dataset [45] (a large dataset with common learnable features to the target dataset) and train it on our target dataset. Our adopted transfer learning framework is summarized into four steps: 1. Installing the layers from a pre-trained model as the ''base model'' on our target classifier, excluding the fully connected layers at the top of its network. 2. Freezing the base model to prevent its weights from being modified. 3. Adding trainable, fully connected layers on top of the frozen base model to turn its features into predictions on our target dataset. 4. Training the (trainable) layers on our new training

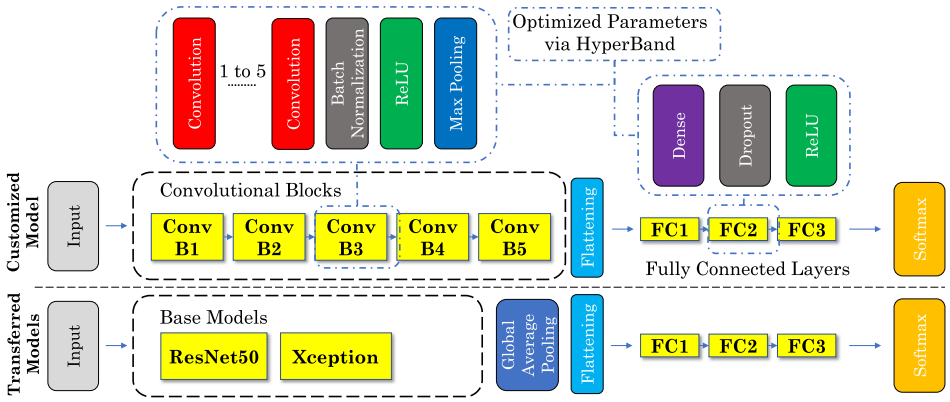

FIGURE 2. The architecture of the CNN-based classifier models. The HyperBand algorithm is used to optimize the number of the convolutional layers (in each Conv B) and the output dimensionalities.

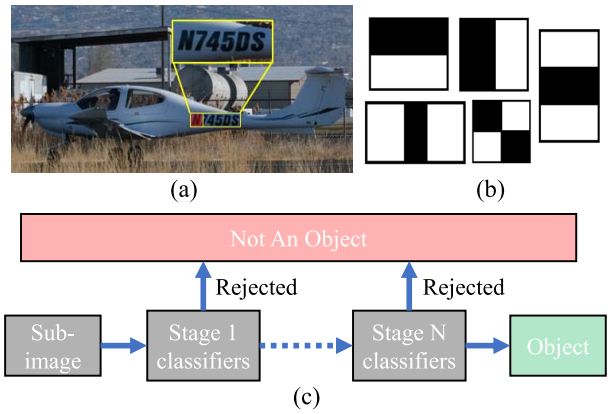

FIGURE 3. (a) N detection; (b) Haar-like features; (c) Haar cascade classifier stages.

dataset. Step 3 comprises a tuning process, similar to the custom model tuning process, to optimally determine the output dimensionality of the fully connected layers (except the last one), improving the performance of the final classifier.

The convolutional layers in the custom classifier model are replaced with a base model in the transferred classifier models (Fig. 2). Then, the flattening layer is preceded by global average pooling to transform the product of the base model's last layer into a 2D feature map representation. In the end, the top fully connected layers scheme is the same as those used for the custom classifier model. We used ResNet50 [34] and Xception [35], two deep neural networks, as the base model for transfer learning.

The reason for this choice is their good performance in terms of accuracy and speed. ResNet50 is constructed based on a residual learning framework, which is originally presented to enable deeper networks with faster inference steps, but without reducing the capacity of the network. On the other hand, Xception is developed with the idea of gaining a higher performance than its counterpart network (i.e., Inception V3 [46]), but without increasing the capacity. This goal is achieved by replacing the regular convolutions in the Inception V3 architecture with depthwise separable convolutions.

B. TAIL NUMBER RECOGNITION

1) TAIL NUMBER DETECTION

We propose a feature-based and rapid tail number detector and compare it with a deep neural network text detector (TextBoxes [47]) for validation. We use Haar cascade classifier [48] to construct the feature-based detector, which is faster than deep neural network text detectors and facilitates real-time application. We chose the TextBoxes algorithm developed by Liao *et al.* [47], which is a popular deep learning text detector.

FAA refers to tail numbers as the N-Number because U.S. aircraft registration numbers start with the letter "N" [49]. With that, once the "N" character is detected, the tail number window is set to the same height as the bounding box of the "N" character. As Fig. 3a indicates, the width of this window is an extended width of the "N" bounding box. The experiments have shown that extending the "N" bounding box width four times accurately encompasses the actual tail number length. Therefore, we construct a feature-based text detector to detect the "N" character in the aircraft image plane using the Haar cascade classifier.

This cascaded method classifies each candidate subwindow of an image in consecutive rejection and acceptance stages; each is structured with a combination of weak classifiers, i.e., Haar-like features (Figures 3b and 3c). Haar-like features are convolved to the subwindow to determine if it contains the object. An Adaboost algorithm is used to optimize the selection of the classifier parameters to increase the hit rate (true positive detection rate) and decrease the false detection rate at each stage. While a minimum hit rate of 0.999 is recommended by Lienhart *et al.* [50], we chose 0.997 as any higher value would significantly decelerate the training process. A maximum false alarm rate of 0.4 proved to be efficient in our experiments.

As for the other hyperparameters related to the degenerate trees of weak classifiers, we fixed the weight trim rate to 0.95, maximal weak tree depth to 1, and maximal weak trees per stage to 100. As suggested in [51], a Gentle Adaboost, which typically enhances the generalization

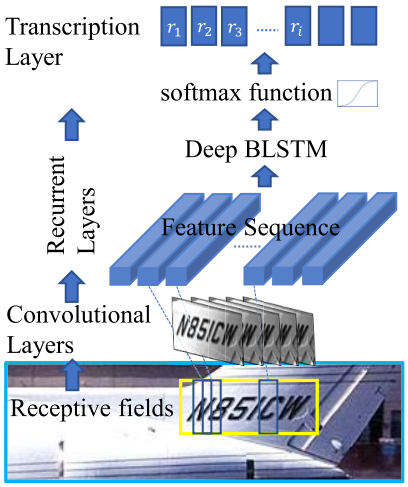

FIGURE 4. The CRNN architecture and how the probability distribution of the recognized label sequences are obtained. Each vector in the feature sequence is associated with a receptive field.

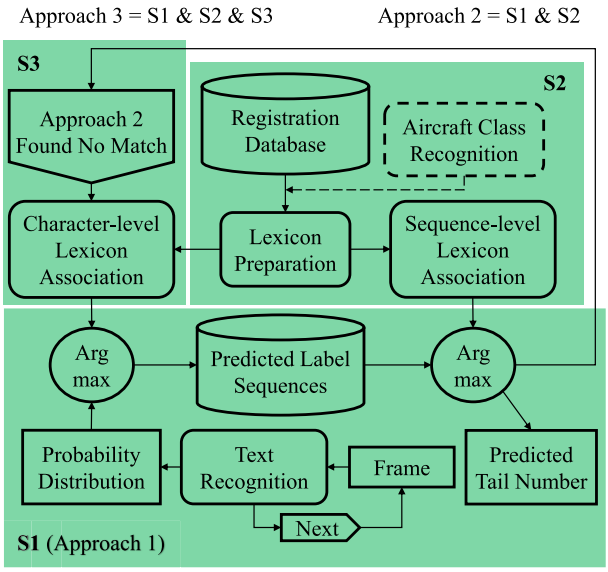

FIGURE 5. Three probabilistic MFB identification approaches.

performance, is used to form the degenerate trees. Finally, a grid search is performed over three maximum number of stages (i.e., 10, 15, and 20) and two sample window sizes (i.e., 20 × 20 and 24 × 24). 248 positive image samples (i.e., images of "N") and 415 negative image samples are extracted from random images retrieved from the web and set as the training data. A validation dataset of 100 aircraft images validated the use of the model with 24 × 24 window sizes for its higher tail number detection rate. The best model continued to train for 15 stages and terminated after achieving the overall false alarm rate criteria (i.e., $\text{MaxFalseAlarmRate}^{\text{MaximumNumberOfStages}}$).

2) TEXT RECOGNITION

We propose three approaches for predicting the aircraft identity, each succeeding approach with incrementally added complexity to the model. All three approaches use a text recognition network with a conditional probability distribution representation of the predicted label sequences.

We use the text recognition model of the convolutional recurrent neural network (CRNN) [52] (structured with convolutional, recurrent, and transcription layers) for its accuracy and speed. The convolutional layer receives the image as the input and outputs feature sequences that are associated with rectangular regions (window) of the input image (Fig. 4). These feature sequences are then fed to recurrent layers to produce per-receptive-field predictions. Each prediction is a score list of all possible character classes, including uppercase English alphabet, numbers, and a blank. The set of character classes is denoted by Ω. The letters I and O are not to be used based on the FAA regulations on forming an N-number to avoid confusion with numbers one and zero [49].

We added a softmax function to this network after the bidirectional long short-term memory (BLSTM) layer in the recurrent layers to normalize the score list of prediction of each window (z_i) to a probability distribution over the predefined character classes,

$$P(r_i = \omega) = \frac{e^{z_{i_k}}}{\sum_{k=1}^{L_r} e^{z_{i_k}}}, \tag{1}$$

where $L_r = |\Omega|$ and ω is an element of set Ω. Lastly, the blanks and repeated labels (overlapped receptive fields) will be removed to determine the final probability distribution of the recognized label sequence for a video frame, $\mathbf{r} = r_1, \ldots, r_{L_s}$, where L_s is the length of the predicted label sequence.

Probabilistic Multi-Frame-Based (MFB) Approaches: For all three approaches, we implement a CRNN model pre-trained on two well-known synthetic text recognition datasets named MJSynth and SynthText [53]. Fig. 5 summarizes the following approaches of aircraft identification.

Approach 1: At each video frame,

$$r_i^* = \arg\max_{\omega \epsilon \Omega} P(r_i = \omega) \tag{2}$$

denotes the most probable value of r_i. Furthermore, $\mathbf{r}^* = r_1^*, \ldots, r_{L_s}^*$ denotes the predicted label sequence for that particular video frame, and $A = \mathbf{r}_1^*, \ldots, \mathbf{r}_{N_f}^*$ denotes the set of predicted label sequences for all video frames, where N_f is the number of selected frames. The first approach ultimately selects the one with the most frequent occurrence during the operation,

$$T_{A1}^* = \arg\max_x |\{x \in A\}|. \tag{3}$$

Approach 2: Here, we alter the first approach by associating the most frequent label sequence argument with a lexicon defined for tail numbers,

$$T_{A2}^* = \arg\max_{x \in \Psi} |\{x \in A\}|, \tag{4}$$

where Ψ denotes the tail number lexicon which is compiled by extracting the list of the registered aircraft tail numbers

that are relevant to the recognized aircraft classes from the database.

Approach 3: The third approach enhances the second approach in cases where there is no actual match between the tail number lexicon and the set of predicted label sequences during the operation time window. Here, the tail number in the lexicon that achieves the highest conditional probability with the observation of r,

$$\mathbf{s}^* = \arg\max_{T^D \epsilon \Psi} p\left(T^D \middle| r\right), \tag{5}$$

is considered as the predicted label sequence for a video frame, and $B = \mathbf{s}_1^*, \ldots, \mathbf{s}_{N_f}^*$ denotes the set of predicted label sequences for all video frames. T^D denotes a tail number listed in the lexicon and

$$p(T^D|r) = \frac{\sum_{j=1}^{N_t} p(r_j|T^D{}_{(j)})}{N_t}, \tag{6}$$

where N_t is the tail number length and $T^D{}_{(j)}$ is the jth character of the target tail number. Finally, we select the most frequently recognized tail number during the operation time window,

$$T_{A3}^* = \arg \max_x |\{x \in B\}|. \tag{7}$$

IV. EXPERIMENTAL SETUP

This section illustrates how we conduct the training of the CNN-based classifiers. Then, we elaborate on actual data collection procedures to evaluate the performance of the proposed identification method.

A. CNN-BASED CLASSIFIERS

1) TRAINING DATA AND CUSTOMIZED AIRCRAFT CLASSES

For training purposes, we use the FGVC-Aircraft image dataset [32] that contains 10,000 aircraft images, with 100 images for each of the 100 model variants. The dataset is organized in a hierarchy based on the model, variant, family, and manufacturer. However, we classify them into aircraft classes that are useful specifically for our proposed identification system. The information available in the FAA-standard registration database governs the definition of functional classes. The releasable database archive file includes the *Aircraft Registration Master file* and *Aircraft Reference file by Make/Model/Series Sequence* [54]. The list of the visually noticeable and perceivable information in database files comprises the aircraft type, engine type, number of the engines, aircraft size (i.e., weight class), and in some cases, the aircraft manufacturing model. Given these details as well as the aircraft models available in the FGVC dataset, we defined 13 classes that encompass aviation fleet mixes at a wide range of airports. Table 1 presents the 13 classes and the criteria by which the proposed method refines the registration database after classifying the operating aircraft into one of these 13 classes.

The differences between reciprocating, 4 cycle, 2 cycle, and rotary engines are mostly in their combustion process;

TABLE 1. Aircraft classes; a sample image from each class is displayed in Fig. 6.

Cls	Features to Refine the Database					Aircraft Models Selected from FGVC Dataset	#Images
	Aircraft Type	Engine Type	Weight Class	#Engine	Manufacturer		
a	Single-Engine	Piston (Reciprocating, 4 Cycle, 2 Cycle, Rotary)	Class 1 & 2	1	-	Cessna 172, DH-82, DHC-1, DR-400, PA-28, SR-20	600
b	Single-Engine	Turbo-prop	Class 1 & 2	1	-	Cessna 208	100
c	Multi-Engine	Turbo-prop & Piston	Class 1 & 2	2	-	Beechcraft 1900, DHC-6, EMB-120, B200	400
d	Multi-Engine	Turbo-prop	Class 3	2	-	ATR-72, DHC-8-300, Fokker 50, Saab 2000	400
e	Multi-Engine	Turbo-fan, Turbo-jet	Class 1 & 2	2	-	BAE-125, Cessna 525, Cessna 560, Falcon 2000	400
f	Multi-Engine	Turbo-fan, Turbo-jet	Class 1 & 2	3	-	Falcon 900	100
g	Multi-Engine	Turbo-fan, Turbo-jet	Class 3	2	-	CRJ-700, CRJ-900, E-170, E-190, E-195, Fokker 100, Tu-134	700
h	Multi-Engine	Turbo-fan, Turbo-jet	Class 3	2	AIRBUS	A300B4, A310, A318, A319, A320, A321, A330-200, A330-300	800
i	Multi-Engine	Turbo-fan, Turbo-jet	Class 3	2	BOEING	737-200/300/400/500/600/700/800/900, 757-200/300, 767-200/300/400, 777-200/300,Boeing 717	1600
j	Multi-Engine	Turbo-fan, Turbo-jet	Class 3	2	EMBRAER BOMBARDIER GULFSTREAM	ERJ 135, ERJ 145, Global Express, Gulfstream IV, Gulfstream V	500
k	Multi-Engine	Turbo-fan, Turbo-jet	Class 3	2	MCDONNEL-DOUGLAS	DC-9-30, MD-80, MD-87, MD-90	400
l	Multi-Engine	Turbo-fan, Turbo-jet	Class 3	3	-	727-200, DC-10, L-1011, MD-11, Tu-154, Yak-42	600
m	Multi-Engine	Turbo-fan, Turbo-jet	Class 3	4	-	707-320, 747-100, 747-200, 747-300, 747-400, A340-200, A340-300, A340-500, A340-600, A380, BAE146-200, BAE146-300,DC-8	1300

Note: Aircraft maximum gross take-off weight in pounds: 1- Up to 12,499; 2- 12,500 - 19,999; 3- 20,000 and over.

therefore, they are placed in the same group. Turbo-prop aircraft generally can carry more payload than piston-powered aircraft. This attribute frequently leads to further appearance differences between them (class a and class b). The same logic applies to differentiating turbo-fan/jet models from turbo-prop models. The absence of propellers in turbo-fan/jet models is another expressive feature. As Fig. 6 illustrates, the number of engines and weight class of aircraft models allow further grouping of models with the same engine type. Finally, we took advantage of the available set of heavy turbo-fan/jet aircraft images in the FGVC-Aircraft dataset to recognize the manufacturer of these aircraft (class h-k). The similarities between the proxies from Embraer, Bombardier, and Gulfstream in the image dataset encouraged us to have them in one class (class j).

2) TRAINING PROCEDURE

We randomly split the selected FGVC-Aircraft images into three sets: training set (66% of data), validation set (17% of data), and test set (17% of data). The loss calculated on the validation set was monitored during model training to select the best-performing model. The images were resized to the default CNN models' input sizes, 224×224 for ResNet50 and 299×299 for Xception, and we chose 256×256 for the custom model. Furthermore, we implemented data augmentation by synthesizing the existing training data. Random horizontal

FIGURE 6. Sample images from aircraft classes based on Table 1.

TABLE 2. The optimum architecture of the CNN-based classifiers.

Variables	Custom Model		Transferred Models	
	# Conv Layers	Output Dimensionalities		
Conv B1	5	16, 48, 16, 16, 48	ResNet50	Xception
Conv B2	2	64, 64		
Conv B3	3	256, 64, 256		
Conv B4	2	512, 256		
Conv B5	4	512, 256, 128, 384		
FC1	-	512	1024	1024
FC2	-	256	512	512
FC3	-	13 (aircraft classes)	13	13
Learning Rate	0.0001		0.0001	0.0001
#Parameters	**18,711,245**		26,217,357	23,491,125

flip and random rotation in the range of $[-\frac{2\pi}{10}, +\frac{2\pi}{10}]$ were applied to each batch of 32 images propagated through the network at each epoch. We applied two regularization strategies to avoid overfitting: kernel-level regularizer using L2 regularizers with the factor of 0.01 for convolutional layers in the custom model, and dropout with the probability of 0.35 for fully connected layers in all three models. We used categorical cross-entropy as the loss function and Adam optimizer to train the classifier models.

The three CNN-based classifiers were optimized to achieve maximum performance by allowing a maximum of 100 epochs training for generated agents (i.e., model configurations) from the predefined search space in section III-A1. The optimum architectures found after the search process (using the HyperBand algorithm) are tabulated in Table 2. The total number of the parameters in the models was bounded by imposing the fixed boundaries for the search space. Interestingly, the number of the parameters of the optimum architecture found for the custom model is close to the mean of all 40 generated agents (Fig. 7).

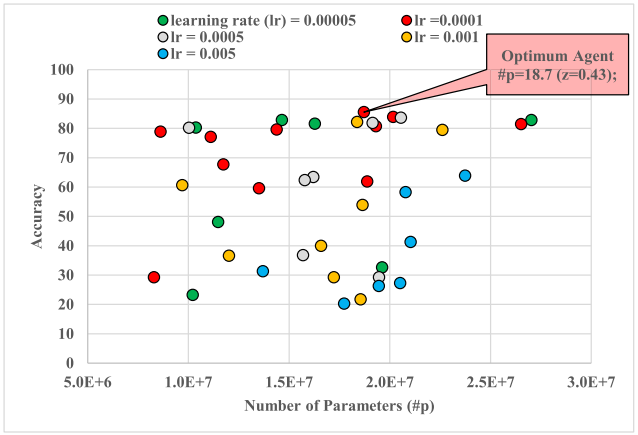

FIGURE 7. 40 generated models for custom CNN-based classifier using the HyperBand algorithm and Keras Tuner (z: the normalized value of the #p).

Next, we continue training each optimized model (which was already trained for 100 epochs) and terminate the training process when the validation loss does not improve for more than 30 epochs. For the transferred models, after having the model converge on the target dataset, we fine-tune the model by unfreezing the base model and continuing the training process in order to utilize the entire model capacity. The learning rate is reduced 10 times during the fine-tuning process to achieve incremental improvements and, at the same time, avoid overfitting.

3) COMPARISON OF THE CNN-BASED CLASSIFIER MODELS

The confusion matrices in Fig. 8 summarize the performance of all three models on the test set of the FGVC-Aircraft dataset using confusion matrices. They illustrate a consistently better performance in classifying heavyweight jet aircraft classes (g-m classes) using the custom classifier model, which exhibits a minimum classification accuracy of 80% (Fig. 8, top). The custom model has a slightly higher rate of false positives for lightweight trijet aircraft (class f) as this aircraft class is confused with twinjet aircraft (class e) in 18% of cases. A potential reason could be the lower number of samples for class f aircraft. Similarly, the unbalanced dataset has potentially caused the slightly higher false-positive rates in detecting single-engine turbo-prop aircraft (class b) for all three classifier models. A portion of misclassifications relates to the adverse effect of possibly predicting the classes with the higher number of image samples. The column "i" in confusion matrices of all three models indicate the impact of the unproportionately larger number of BOEING image samples, especially on the Xception model with a total false-positive rate of 47% (Fig. 8, bottom).

As Fig. 9 shows, applying each of the three classifier models to the test set allows the top 3 predicted classes to secure more than 96% accuracy. Thus, we consider the top-3 recognized classes (after applying the classifier to the detected aircraft in selected video frames from the operation time window) when filtering the registration database.

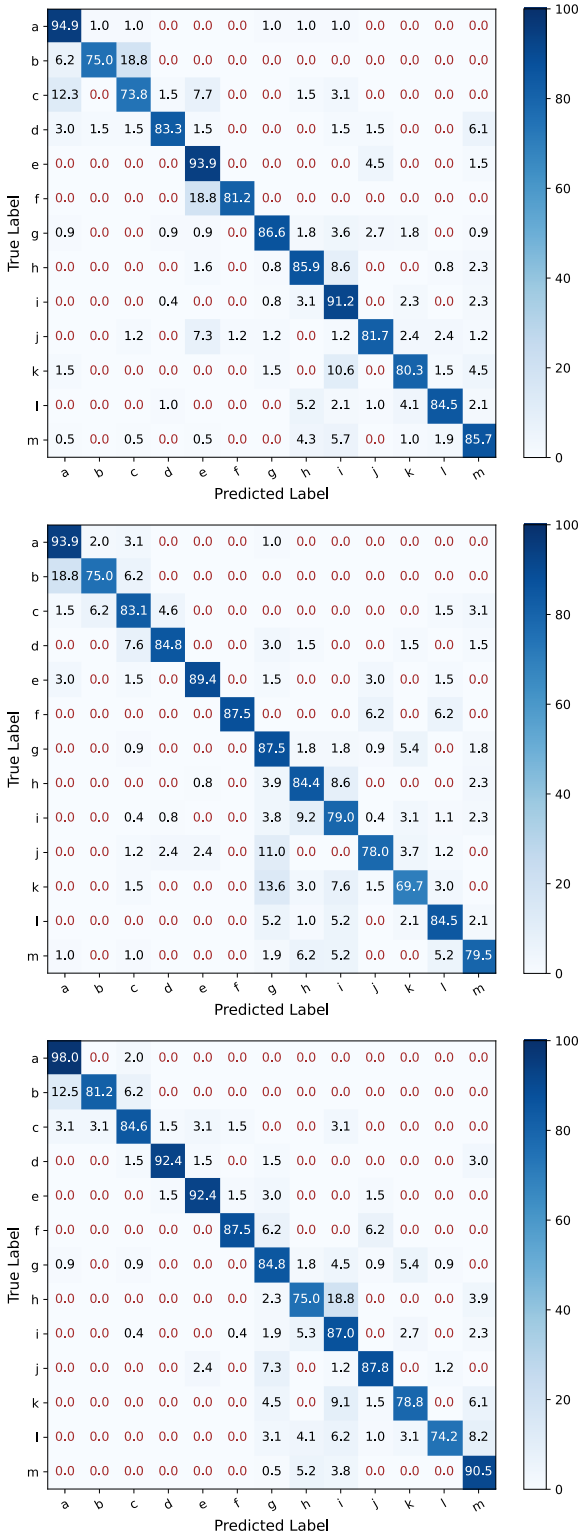

FIGURE 8. Confusion matrices for classification results on the test set of FGVC-Aircraft dataset. **Top:** Custom CNN; **Middle:** Transferred ResNet50; **Bottom:** Transferred Xception.

It minimizes the chance of eliminating the actual tail number from the database. Top-3 accuracy is the accuracy where the true class matches with any one of the 3 most probable classes

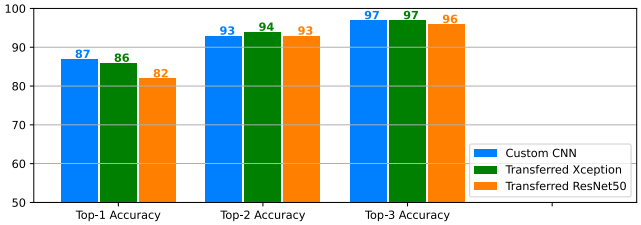

FIGURE 9. Accuracy for classification results on the test set of FGVC-Aircraft dataset (Top-"n" accuracy is the accuracy where the true class matches with any one of the "n" most probable classes predicted by the model).

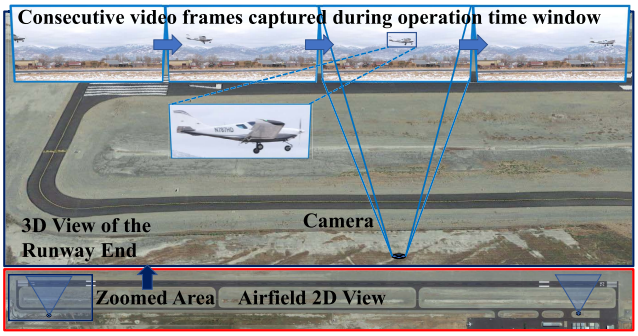

FIGURE 10. Camera layout and field of view for a runway on an airport layout plan.

predicted by the model. We selected the *custom classifier model* for use in the proposed identification system for its fewer parameters (faster inference), lower loss, higher accuracy, and slightly more consistent recognition performance for the individual aircraft classes.

B. DATA COLLECTION FROM AIRFIELD

The model performance is explored on data collected at three general aviation airports in Utah: Bountiful Airport, Heber Valley Airport, and Brigham City Municipal Airport. The airports' runways ranged from moderately short to long runways with lengths of 4,700 ft, 6,800 ft, and 8,800 ft, respectively. The three airports allowed us to have various aircraft models in our collected data, which warranted different aircraft approach speeds. We used commercial off-the-shelf digital cameras (Fuji Film and GoPro) and recorded the video data with 3120 × 1760 resolution. The data is collected in several sessions in the daytime on sunny, overcast, and snowy days. Under adverse weather conditions, aircraft classification is expected to work, but the visibility of tail numbers can be affected.

Fig. 10 exhibits a schematic display of the camera layout and cameras' positioning and field of view at one end of the airport. With runway safety area considerations, two cameras are located at each end of the runway and oriented toward the runway ends, capturing the landing aircraft off the runway surface level while approaching the airport. These cameras capture the departure operations on the runway surface level because aircraft pilots run from the end of the runway for take-off. This measure adds a safety margin for a stop on

(a) Departure (b) Short Landing (c) Moderately Long Landing (d) Very Long Landing

FIGURE 11. Examples of departure and different landing approaches in collected data from airfield.

the runway in case of an engine failure or rejected take-off. In the case of multiple runways, each runway would require a separate set of cameras.

To validate the occurrence of the operations, we assigned the two ends of the runway and entrance taxiways to human observers who documented the traffic via visual inspection and by monitoring the pilots' radio communications on the airport common traffic advisory frequency (CTAF). The designated camera setup successfully captured all 141 flight operations during the experimental data collection sessions. The operations comprised departures as well as all landing approach behaviors, including short to long landings (Fig. 11). There were quite a few long landings related to training-related touch-and-go activities.

In this experiment, we used the database of Utah-registered aircraft (released by FAA) and added the tail numbers of the out-of-state aircraft that were previously recorded in the database of test airports. The database was comprised of 7,800 registered aircraft.

V. RESULTS

We evaluate performance of the proposed system by applying our algorithms to 2,351 frames extracted (every 0.1 seconds) from video data of 141 aircraft operations (as stated in section III).

A. PERFORMANCE OF TAIL NUMBER DETECTION AND TEXT RECOGNITION

To evaluate the performance of the proposed tail number detection method, we used precision and recall calculated by computing the similarity of the predicted bounding boxes to their associated ground truth using the value of their intersection over union. Table 3 shows that the developed tail number detection using Haar cascade is remarkably faster than the TextBoxes and appropriate for a real-time system. Despite the significant difference in their processing times, the accuracy of both detectors is high and only moderately apart, with the minor superiority of the TextBoxes. The major reason was the occlusion of the letter "N" by the aircraft wing at some frames during the operation.

On average, 67% of the individual tail number characters are correctly recognized by applying the CRNN (text recognition algorithm) to the detected tail number image boxes in the video frames of each operation. The actual tail numbers are obtained by reviewing the video and matching human observations with the notes taken during in-field data collection sessions. Errors in tail number detections and character recognitions mainly stemmed from the small sizes or skewness of tail numbers characters as well as the blur caused by fast-moving aircraft.

TABLE 3. Performance of the tail number detection methods tested on 2,351 video frames of 141 aircraft operations.

Algorithm	Processing time	Precision	Recall
Haar Cascade (feature-based "N" detector)	11 milliseconds	0.84	0.77
TextBoxes (deep neural network text detector)	203 milliseconds	0.91	0.83

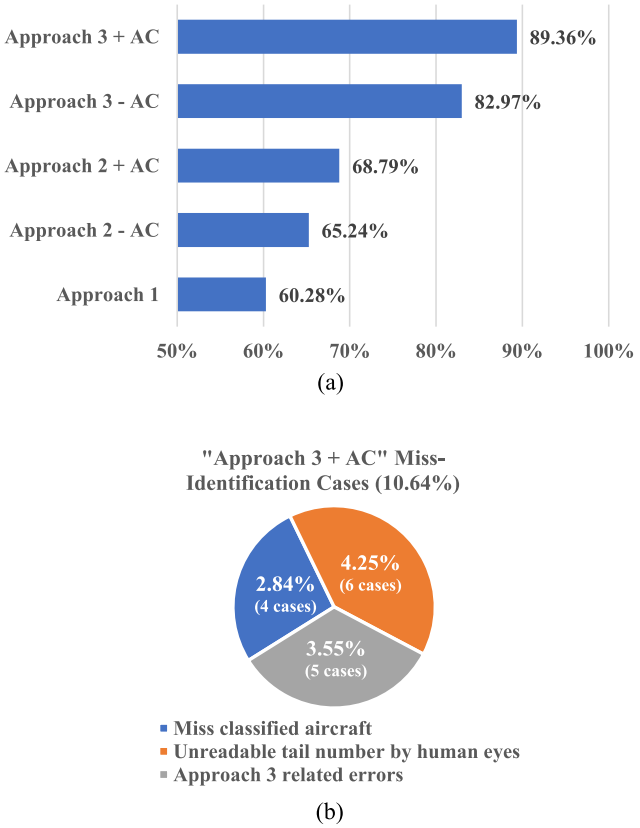

FIGURE 12. (a) Aircraft identification accuracy on collected data from airfield (+ AC: with aircraft classification, − AC: without aircraft classification); (b) Miss-identification cases.

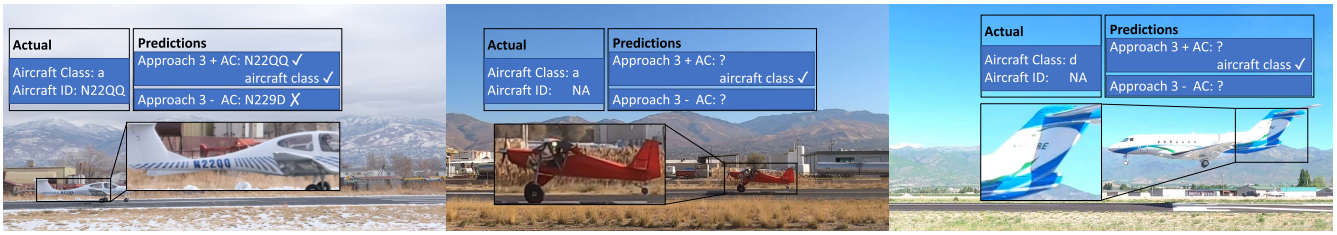

FIGURE 13. Two-step identification versus identification without classification for two general aviation aircraft (+ AC: with aircraft classification, − AC: without aircraft classification); (a) difficult-to-read tail number; (b) no imprinted tail number; (c) tail number visibility affected by illumination.

B. PERFORMANCE OF AIRCRAFT IDENTIFICATION WITH COMPONENT ANALYSIS

Despite the CRNN limited accuracy for recognizing individual characters of the aircraft tail number in the video frames of each operation, the identification approaches predicted the actual tail number of operations with an incremental improvement in each succeeding approach. Fig. 12a shows that approach 3 with aircraft classification (*two-step identification*) resulted in the highest accuracy for predicting the actual tail numbers in 141 operations. Approach 1, which finds the most frequently predicted label sequence with no lexical constraint, achieved the lowest accuracy. Approach 2 increased accuracy by associating the tail number lexicon with sequence recognition in the identification process, with an additionally increased accuracy using aircraft classification. After observing the CRNN results, the proposed approach 3 (the most completed probabilistic MFB approach in our framework) corrected a considerable portion of the miss-identifications of approach 2.

The aircraft classification module played a significant role in the reliability of the proposed identification method. The CNN-based custom classifier model successfully predicted the class of 97.16% (137 out of 141) operating aircraft in the top-3 predictions. The consistency of the top-3 accuracies for both the FGVC-Aircraft image test set (Fig. 9) and the collected video data from airfield (Fig. 12b) indicates the high generalizability of the classifier model, which stems from the applied effective regularization. Fig. 12 shows that even though the classification module miss-classified 2.84% of the operating aircraft, it increased the overall identification accuracy of the third approach from 82.97% to 89.36% by removing irrelevant tail numbers from the search space in the database. On average, the two-step method reduced the search space in the database by 56%. The classification module could be even more helpful in the case of a larger database where it would help filter even more irrelevant tail numbers.

The two-step method alleviates disparities between the text recognition results that stem from noises in the tail number images by removing many irrelevant but potentially similar tail numbers (Fig. 13a). Having a close estimation of the operating aircraft class is another benefit, especially where the identification module fails. Examples include the cases where the aircraft has no imprinted tail number or the tail number is unreadable. In this particular study, the classifier

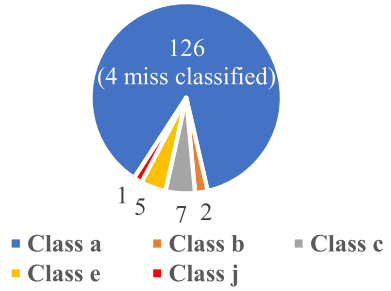

FIGURE 14. Each class quantification in the captured video data.

correctly recognized the top 3 classes of 73% miss-identified aircraft (Figures 12b, 13b, and 13c).

It is noteworthy that "class a" aircraft was the prevalent class in the collected video data, thereby adding more difficulty to the identification task due to the higher variations in the appearance of these aircraft tail numbers. Specifically, our collected video data mainly contains operations of the general aviation fleet, which comprises more than 90% of the registered civil aviation aircraft in the US [13]. These aircraft types typically operate in airports that are outside of the airspace where ADS-B enabled avionics are required [1], increasing the usability of a vision-based system as an alternative solution. As Fig. 14 illustrates, aircraft classes in our collected video data comprise class a, b, c, e, and j. Interestingly, all captured aircraft classes b, c, e, and j are correctly classified.

C. PROCESSING TIMES

The computational experiments in this paper are benchmarked on a 64-bit Windows Operating System with a 3.20 GHz IntelR Core(i7) CPU. The CPU-only inference closely estimates the system's performance for compiling the system on low-cost processing platforms such as single-board computers for edge computing. We observe the total processing time of 122 milliseconds per frame during the operation time window (i.e., tracking aircraft and recognition of the target aircraft class and its tail number). Since this is close to our extraction rate of video frames (every 0.1 seconds), we conclude that the proposed system can be used in near-real-time using an affordable processing platform. Furthermore, aircraft classification reduced the processing time of the final identification by approximately 50%.

FIGURE 15. Extracted video frames from the proposed video-based identification system for two operations; aircraft identity is predicted using the two-step approach 3 once the aircraft exit the field of view.

Fig. 15 exhibits the extracted video frames from the proposed video-based aircraft identification system.

VI. DISCUSSION

The proposed two-step method has shown to be an effective approach for identifying general aviation aircraft. The collected data contained many challenges regarding aircraft identification, including many tail numbers that were difficult to read due to small fonts, inclined fonts, and blurred images. Moreover, the MFB framework is proved to be superior to single-shot detection because using only a subset of the frames leads to misidentification due to reduced or obstructed visibility.

Any vision-based system may underperform at nighttime. Nevertheless, nighttime operations are rare at non-towered airports. Also, airports that expect significant nighttime operations may still use the proposed system in conjunction with appropriate lighting or night-vision cameras. Additionally, the minimum required visibility for landing aircraft in airports exceeds the distance between the camera position in our setting and the operating aircraft on the runway.

The proposed classification scheme is designed to cover a wide range of airports with various fleet mixes, including general aviation fleet and large airliners. That said, other classification schemes might work better for specific airports, e.g., commercial service, general aviation, or cargo service airports. In those cases, the availability of the training images and visually perceivable information (aircraft specifications) in the registration database would help determine the best classification scheme.

The proposed vision-based system can assist in automating the billing process associated with landing fees in

non-towered airports. This application has not been considered in the previous works [10], [11]. Moreover, unlike the ADS-B-based approaches [17], our proposed method can identify non-cooperative aircraft.

VII. CONCLUSION

This paper presented a two-step computer vision-based system for aircraft identification, which first recognizes the aircraft class and then its tail number. The former task is based on a customized CNN classifier and it helps reduce the search space in the FAA database to find the target tail number. The latter task integrates results of a text recognition algorithm into a probabilistic MFB framework whose performance is further enhanced by leveraging the FAA registration databases. Importantly, the proposed system efficiently covers all-type aircraft operations, i.e., departure, landing, and training-related touch-and-go, through the cameras deployed at each end of the runway.

The proposed method is tested on data collected from three general aviation airports. The aircraft classification with the lexical probabilistic string analysis proved to be an accurate and reliable approach for identifying operating aircraft. Despite limited accuracy in recognizing individual characters in the aircraft tail number, the proposed two-step identification approach successfully identified approximately 90% of the aircraft. The future research path would be to leverage a secondary data source (e.g., ADS-B) to further increase accuracy of the vision-based system.

REFERENCES

[1] M. J. Muia and M. E. Johnson, *Evaluating Methods for Counting Aircraft Operations at Non-Towered Airports*. Transportation Research Board: Washington, DC, USA, 2015.
[2] J. H. Mott, M. L. McNamara, and D. M. Bullock, "Estimation of aircraft operations at airports using nontraditional statistical approaches," in *Proc. IEEE Aerosp. Conf.*, Mar. 2016, pp. 1–11.
[3] Air Safety Institute. (2020). *Operations at Nontowered Airports*. Accessed: Oct. 1, 2020. [Online]. Available: https://www.aopa.org/-/media/files/aopa/home/pilot-resources/asi/safety-advisors/sa08.pdf?la=en
[4] Q. Zhang, J. H. Mott, M. E. Johnson, and J. A. Springer, "Development of a reliable method for general aviation flight phase identification," *IEEE Trans. Intell. Transp. Syst.*, early access, Aug. 30, 2021, doi: 10.1109/TITS.2021.3106774.
[5] X. Chen, M. Yi, and J. Huang, "Application of a PCA-ANN based cost prediction model for general aviation aircraft," *IEEE Access*, vol. 8, pp. 130124–130135, 2020.
[6] I. V. Pustokhina, D. A. Pustokhin, J. J. P. C. Rodrigues, D. Gupta, A. Khanna, K. Shankar, and G. P. Joshi, "Automatic vehicle license plate recognition using optimal K-means with convolutional neural network for intelligent transportation systems," *IEEE Access*, vol. 8, pp. 92907–92917, 2020.
[7] Z. Gui and H. Li, "Automated defect detection and visualization for the robotic airport runway inspection," *IEEE Access*, vol. 8, pp. 76100–76107, 2020.
[8] Y. Han, S. Ma, Y. Xu, L. He, S. Li, and M. Zhu, "Effective complex airport object detection in remote sensing images based on improved end-to-end convolutional neural network," *IEEE Access*, vol. 8, pp. 172652–172663, 2020.
[9] T. V. Phat, S. Alam, N. Lilith, P. N. Tran, and N. T. Binh, "Deep4Air: A novel deep learning framework for airport airside surveillance," in *Proc. IEEE Int. Conf. Multimedia Expo Workshops (ICMEW)*, Jul. 2021, pp. 1–6.
[10] J. M. Molina, J. Garcia, A. Berlanga, J. Besada, and J. Portillo, "Automatic video system for aircraft identification," in *Proc. 5th Int. Conf. Inf. Fusion (FUSION)*, vol. 2, 2002, pp. 1387–1394.
[11] D. G. Vidakis and D. I. Kosmopoulos, "Facilitation of air traffic control via optical character recognition-based aircraft registration number extraction," *IET Intell. Transp. Syst.*, vol. 12, no. 8, pp. 965–975, Oct. 2018.
[12] International Civil Aviation Organization. (1981). *Convention on Civil Aviation*. Accessed: Jan. 1, 2021. [Online]. Available: https://www.icao.int
[13] Aircraft Owners and Pilots Association. (2019). *State of General Aviation*. Accessed: Mar. 1, 2021. [Online]. Available: https://download.aopa.org/hr/Report_on_General_Aviation_Trends.pdf
[14] M. Farhadmanesh. (2021). *General Aviation Aircraft and Registration Number Labeled Image Dataset*. Mendeley Data. [Online]. Available: https://data.mendeley.com/datasets/f9ft69jgw6/2
[15] J. H. Mott and N. A. Sambado, "Evaluation of acoustic devices for measuring airport operations counts," *Transp. Res. Rec., J. Transp. Res. Board*, vol. 2673, no. 1, pp. 17–25, Jan. 2019.
[16] Florida Department of Transportation. (2018). *Operations Counting at Non-Towered Airports Assessment*. Accessed: Feb. 4, 2021. [Online]. Available: http://www.invisibleintelligencellc.com/uploads/1/8/4/9/18495640/2018_ops_count_project_final_report_09102018.pdf
[17] J. H. Mott, "Measurement of airport operations using a low-cost transponder data system," *J. Air Transp.*, vol. 26, no. 4, pp. 147–156, Oct. 2018.
[18] C. Yang, "Leveraging aircraft transponder signals for measuring aircraft fleet mix at non-towered airports," *Int. J. Aviation, Aeronaut., Aerosp.*, vol. 8, no. 2, p. 1, 2021.
[19] Federal Aviation Administration. (2021). *ADS-B in and Out, Installation*. Accessed: May 17, 2021. [Online]. Available: https://www.faa.gov/nextgen/equipadsb/installation/
[20] C. Yang, J. H. Mott, B. Hardin, S. Zehr, and D. M. Bullock, "Technology assessment to improve operations counts at non-towered airports," *Transp. Res. Rec., J. Transp. Res. Board*, vol. 2673, no. 3, pp. 44–50, Mar. 2019.
[21] Federal Aviation Administration. (2021). *Runway Safety Statistics*. Accessed: Jan. 7, 2021. [Online]. Available: https://www.faa.gov/airports/runway_safety/statistics/
[22] M. Farhadmanesh, A. Rashidi, and N. Marković, "Implementing Haar cascade classifiers for automated rapid detection of light aircrafts at local airports," in *Computing in Civil Engineering: Data, Sensing, and Analytics*. Reston, Virginia, USA: American Society of Civil Engineers, 2021.
[23] M. Farhadmanesh, N. Marković, and A. Rashidi, "An Automated Video-Based Air Traffic Surveillance System for Counting General Aviation Aircraft Operations at Non-Towered Airports," unpublished.
[24] J. Straub, "Application of an image feature network-based object recognition algorithm to aircraft detection and classification," in *Automatic Target Recognition*, vol. 9090. Bellingham, WA, USA: SPIE, 2014, Art. no. 909005.
[25] Y. LeCun, Y. Bengio, and G. Hinton, "Deep learning," *Nature*, vol. 521, no. 7553, pp. 436–444, May 2015.
[26] Y. Yan, Y. Zhang, and N. Su, "A novel data augmentation method for detection of specific aircraft in remote sensing RGB images," *IEEE Access*, vol. 7, pp. 56051–56061, 2019.
[27] Z.-Z. Wu, S.-H. Wan, X.-F. Wang, M. Tan, L. Zou, X.-L. Li, and Y. Chen, "A benchmark data set for aircraft type recognition from remote sensing images," *Appl. Soft Comput.*, vol. 89, Apr. 2020, Art. no. 106132.
[28] Z.-Z. Wu, T. Weise, Y. Wang, and Y. Wang, "Convolutional neural network based weakly supervised learning for aircraft detection from remote sensing image," *IEEE Access*, vol. 8, pp. 158097–158106, 2020.
[29] T. Van Phat, S. Alam, N. Lilith, P. N. Tran, and B. T. Nguyen, "Aircraft push-back prediction and turnaround monitoring by vision-based object detection and activity identification,"in *Proc. 10th SESAR Innov. Days*. Brussels, Belgium, Tech. Rep., Dec. 2020.
[30] F. Saghafi, S. M. Khansarizadeh, and V. Etminanbakhsh, "Aircraft visual identification by neural networks," *J. Aerosp. Sci. Technol. (JAST)*, vol. 5, pp. 123–128, no. 3, 2008.
[31] S. Z. Ali and M. A. Choudhry, "A generalized higher order neural network for aircraft recognition in a video docking system," *Neural Comput. Appl.*, vol. 19, no. 1, pp. 21–32, Feb. 2010.
[32] S. Maji, E. Rahtu, J. Kannala, M. Blaschko, and A. Vedaldi, "Fine-grained visual classification of aircraft," 2013, *arXiv:1306.5151*.
[33] M. Tan and Q. Le, "EfficientNet: Rethinking model scaling for convolutional neural networks," in *Proc. Int. Conf. Mach. Learn.*, 2019, pp. 6105–6114.
[34] K. He, X. Zhang, S. Ren, and J. Sun, "Deep residual learning for image recognition," in *Proc. IEEE Conf. Comput. Vis. Pattern Recognit. (CVPR)*, Jun. 2016, pp. 770–778.
[35] F. Chollet, "Xception: Deep learning with depthwise separable convolutions," in *Proc. IEEE Conf. Comput. Vis. Pattern Recognit. (CVPR)*, Jul. 2017, pp. 1251–1258.

[36] D. Bloisi, L. Iocchi, D. Nardi, M. Fiorini, and G. Graziano, "Ground traffic surveillance system for air traffic control," in *Proc. 12th Int. Conf. Telecommun.*, Nov. 2012, pp. 135–139.
[37] J. A. Besada, J. M. Molina, J. García, A. Berlanga, and J. Portillo, "Aircraft identification integrated into an airport surface surveillance video system," *Mach. Vis. Appl.*, vol. 15, no. 3, pp. 164–171, Jul. 2004.
[38] A. Berlanga, J. Garcia-Herrero, J. M. Molina, J. Besada, and J. Portillo, "OCR parameters tuning by means of evolution strategies for aircraft's tail number recognition," in *Proc. Congr. Evol. Comput. (CEC)*, vol. 1, 2002, pp. 902–907.
[39] M. Farhadmanesh, A. Rashidi, and N. Marković, "An image processing method for light aircraft tail number detection in general aviation airports," in *Prroc. 101th Annu. Meeting Transp. Res. Board*. Washington, DC, USA, 2022.
[40] Vector. (2021). *Vantage*. Accessed: May 7, 2021. [Online]. Available: https://www.vector-us.com/vantage
[41] Vaxtor. (2021). *Vaxocr*. Accessed: May 7, 2021. [Online]. Available: https://www.vaxtor.com/products/vaxocr/tailfin/
[42] L. Li, K. Jamieson, G. DeSalvo, A. Rostamizadeh, and A. Talwalkar, "Hyperband: A novel bandit-based approach to hyperparameter optimization," *J. Mach. Learn. Res.*, vol. 18, no. 1, pp. 6765–6816, 2017.
[43] T. O'Malley, E. Bursztein, J. Long, F. Chollet, H. Jin, and L. Invernizzi. (2019). *Kerastuner*. [Online]. Available: https://github.com/keras-team/keras-tuner
[44] S. Ioffe and C. Szegedy, "Batch normalization: Accelerating deep network training by reducing internal covariate shift," in *Proc. Int. Conf. Mach. Learn.*, 2015, pp. 448–456.
[45] J. Deng, W. Dong, R. Socher, L.-J. Li, K. Li, and L. Fei-Fei, "ImageNet: A large-scale hierarchical image database," in *Proc. IEEE Conf. Comput. Vis. Pattern Recognit.*, Jun. 2009, pp. 248–255.
[46] C. Szegedy, V. Vanhoucke, S. Ioffe, J. Shlens, and Z. Wojna, "Rethinking the inception architecture for computer vision," in *Proc. IEEE Conf. Comput. Vis. Pattern Recognit. (CVPR)*, Jun. 2016, pp. 2818–2826.
[47] M. Liao, B. Shi, X. Bai, X. Wang, and W. Liu, "TextBoxes: A fast text detector with a single deep neural network," in *Proc. 31st AAAI Conf. Artif. Intell.*, 2017, pp. 1–7.
[48] P. Viola and M. Jones, "Rapid object detection using a boosted cascade of simple features," in *Proc. IEEE Comput. Soc. Conf. Comput. Vis. Pattern Recognit. (CVPR)*, vol. 1, Dec. 2001, p. 1.
[49] Federal Aviation Administration. (2021). *Aircraft Registration; Forming an N-Number*. Accessed: May 12, 2021. [Online]. Available: https://www.faa.gov/licenses_certificates/aircraft_certification/aircraft_registry/forming_nnumber/
[50] R. Lienhart, A. Kuranov, and V. Pisarevsky, "Empirical analysis of detection cascades of boosted classifiers for rapid object detection," in *Proc. Pattern Recognit. Symp.* Berlin, Germany: Springer, 2003, pp. 297–304.
[51] A. AbdelRaouf, C. A. Higgins, T. Pridmore, and M. I. Khalil, "Arabic character recognition using a Haar cascade classifier approach (HCC)," *Pattern Anal. Appl.*, vol. 19, no. 2, pp. 411–426, May 2016.
[52] B. Shi, X. Bai, and C. Yao, "An end-to-end trainable neural network for image-based sequence recognition and its application to scene text recognition," *IEEE Trans. Pattern Anal. Mach. Intell.*, vol. 39, no. 11, pp. 2298–2304, Nov. 2016.
[53] J. Baek, G. Kim, J. Lee, S. Park, D. Han, S. Yun, S. J. Oh, and H. Lee, "What is wrong with scene text recognition model comparisons? Dataset and model analysis," in *Proc. IEEE/CVF Int. Conf. Comput. Vis. (ICCV)*, Oct. 2019, pp. 4715–4723.
[54] Federal Aviation Administration. (2021). *Releasable Aircraft Database*. Accessed: Jan. 12, 2021. [Online]. Available: https://www.faa.gov/licenses_certificates/aircraft_certification/aircraft_registry/releasable_aircraft_download/

MOHAMMAD FARHADMANESH received the B.S. and M.S. degrees in civil engineering from the Iran University of Science and Technology, Tehran, Iran, in 2014 and 2017, respectively. He is currently pursuing the Ph.D. degree in civil engineering with the Department of Civil and Environmental Engineering, The University of Utah. His research interests include machine learning, computer vision, and image processing.

ABBAS RASHIDI (Member, IEEE) received the M.S. degree in civil and environmental engineering from Tehran Polytechnic, in 2004, the M.S. degree in electrical and computer engineering from Georgia Tech, in 2013, and the Ph.D. degree in civil and environmental engineering from Georgia Tech, in 2014.

His dual background in civil engineering and electrical and computer engineering, has enabled him to conduct multidisciplinary research and to implement electrical engineering tools and computational techniques to solve complex civil engineering problems. In particular, he is interested in applying audio/image/video processing techniques to analyze and model complex civil engineering systems. He currently serves as a member for several professional committees, including the Signal Processing in Acoustics Committee of the Acoustical Society of America and the Data Sensing and Analysis (DSA) Committee of the American Society of Civil Engineers (ASCE). He is an Associate Editor and a member of the Editorial Board of two ASCE journals, such as *Journal of Construction Engineering and Management* (ASCE) and *Journal of Performance of Constructed Facilities* (ASCE).

NIKOLA MARKOVIĆ received the B.S. degree in transportation engineering from the University of Belgrade, Serbia, in 2009, and the Ph.D. degree in transportation engineering from the University of Maryland, College Park, MD, USA, in 2013. He is currently an Assistant Professor of civil and environmental engineering at The University of Utah. His research uses operations research and data science to improve the efficiency of transportation systems. His current research is supported by two National Science Foundation grants. He was a recipient of the 2015 Glover-Klingman Prize.